Inorganic Chemistry

Article

pubs.acs.org/IC

Molecular Structure and Vibrational Spectra of Mixed $MDyX_4$ (M = Li, Na, K, Rb, Cs; X = F, Cl, Br, I) Vapor Complexes: A Computational and Matrix-Isolation Infrared Spectroscopic Study

Cornelis Petrus Groen,[†,§] Attila Kovács,*[,†,‡] Zoltán Varga,[†] and Magdolna Hargittai*[,†]

[†]Materials Structure and Modeling Research Group of the Hungarian Academy of Sciences, Budapest University of Technology and Economics, H-1111 Budapest, Szt. Gellért tér 4, Hungary

[‡]European Commission, Joint Research Centre, Institute for Transuranium Elements, P.O. Box 2340, 76125 Karlsruhe, Germany

Supporting Information

ABSTRACT: The structures, energetic, and vibrational properties of $MDyX_4$ (M = Li, Na, K, Rb, Cs; X = F, Cl, Br, I) mixed alkali halide/dysprosium halide complexes have been investigated by a joint computational and experimental, matrix-isolation Fourier-transform infrared spectroscopic (MI-IR), study. According to our DFT computations for the complexes with heavier halides and alkali metals the ground-state structure is the tridentate isomer; while at high temperatures the bidentate structural isomer dominates. The survey of various dissociation processes revealed the preference of the dissociation to neutral MX and DyX_3 fragments over ionic and radical dissociation products. Cationic complexes are considerably less stable at 1000 K than the neutral complexes, and they prefer to dissociate to $M^+ + DyX_4^•$ fragments. The vapor species of selected mixtures of NaBr and CsBr with $DyBr_3$ and of CsI with DyI_3 in the temperature range 900−1000 K have been isolated in krypton and xenon matrices and investigated by infrared spectroscopy. Besides the characteristic vibrational frequencies of the monomeric and dimeric alkali halide species and of the dysprosium trihalide molecules, certain signals indicated the formation of $MDyX_4$ (M = Na, Cs; X = Br, I) mixed complexes. Comparison with the computed vibrational and thermodynamic characteristics of the relevant species lead to the conclusion that these complexes appear in the vapor predominantly as the C_{2v}-symmetry bidentate isomer. This is the first time that this structure was identified in an experimental vibrational spectroscopic study. The signals appearing upon performing a thermal anneal cycle were tentatively assigned to the double complex M_2DyX_5 (M = Na, Cs; X = Br, I). A structure in which one alkali atom is bound to dysprosium by three and the other by two bridges is proposed for these double complexes.

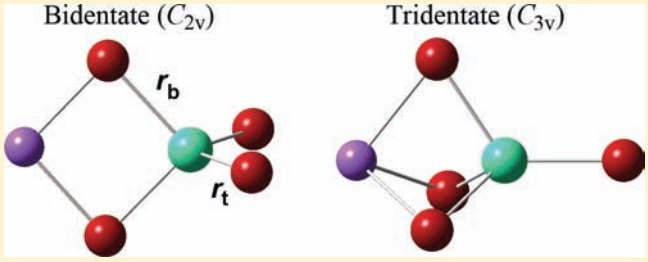

INTRODUCTION

Lanthanide halides (LnX_3, Ln = lanthanide atom, X = halogen) and alkali halides (MX, M = alkali metal) are known to form $MLnX_4$-type mixed complexes in the vapor phase. The existence of these complexes has been shown and thermodynamic characteristics of their dissociation to LnX_3 and MX have been determined by numerous experimental studies, mostly by Knudsen-effusion mass spectrometry.[1−10] Other techniques, such as gas-phase spectrophotometry,[11] torsion-mass-effusion, chemical analysis of the condensed equilibrium vapors, vapor transpiration techniques and vapor pressure measurements have also been applied to a lesser extent (see ref 1 and references therein).

It has been known for a long time[12−15] that complex formation increases the partial pressure of the lanthanide trihalide in the vapor resulting in several practical applications of these complex halides. A variety of bromide and iodide complexes are important vapor species in high-intensity metal halide lamps as they are responsible for the vapor transport of the lanthanide elements from the cooler regions in these lamps to the emitting arc (see, e.g., ref 2). The chloride complexes, on the other hand, were suggested for high-temperature extraction and separation of the lanthanide metals.[16,17]

Optimizing the conditions of high-temperature applications, in particular those in metal halide lamps, often involves thermodynamic modeling. The reliability of this approach depends on the availability of accurate thermodynamic functions of all chemical species involved. For this, the knowledge of their molecular structure and vibrational frequencies is needed—but their experimental determination is hindered by the high temperatures and complex vapor compositions. Therefore, no experimentally determined structure of any $MLnX_4$ complex is available, and only a single vibrational spectroscopic (matrix isolation infrared) study has been reported on $MCl−NdCl_3$ (M = Li, Na, Cs) mixtures and the $LiBr−DyBr_3$ system.[18] Only one IR-active stretching mode of the LnX_4 tetrahedron of $MLnX_4$ (from the altogether 12 fundamentals) was reported,

Received: September 14, 2011
Published: December 2, 2011

 © 2011 American Chemical Society dx.doi.org/10.1021/ic202009v | Inorg. Chem. 2012, 51, 543−556

but no conclusion regarding the molecular symmetry of the complexes could be made. Gas electron diffraction and gas-phase Raman spectroscopic studies on related light rare earth species $KYCl_4$[19] and $CsScI_4$,[4] respectively, did not provide any unambiguous structural assignment either.

The need for accurate thermodynamic functions for the $MLnX_4$ complexes is also illustrated by the available experimental thermodynamic data on these systems reported thus far. Most studies report the enthalpy and entropy of the formation reaction of the respective complex at the average temperature of the experiments (see ref 1 and references therein). This makes a comparison of the formation characteristics of the variations in the alkali, lanthanide and halogen series difficult. The extrapolation of the thermodynamic quantities to T = 298.15 K can only be done when the thermodynamic functions of the respective species are known.

Because of the experimental difficulties with these complex halides, the importance of quantum chemical computations is obvious.[20] Nonetheless, the number of papers reporting computed data on $MLnX_4$ complexes is quite small. Pioneering calculations at the Hartree−Fock level of theory were performed by Kapala et al. on $NaCeCl_4$ and $NaNdCl_4$.[6,21] Beside the simple theoretical level applied, another limitation of this study was that the authors considered only the bidentate structure. Systematic studies using advanced theoretical levels have been performed on $LiLnX_4$ complexes (Ln = La, Ce, Dy; X = F, Cl, Br, I)[22,23] and $MLaX_4$ complexes (M = Na, K, Cs; X = F, Cl, Br, I)[24] as well as on $NaDyBr_4$.[25,26] From these studies, trends in the energetic, structural, bonding, and vibrational properties have been established within the lanthanide series, as well as in the alkali and halogen groups. It has been shown, among others, that the alkali metal−LnX_4 interaction is strongly ionic in these complexes, as the natural charges of the alkali metals are larger than +0.9 e, while those of the interacting halogens are between −0.74 and −0.92 e.[23−25] Some properties of the ionized complex were investigated earlier for $NaDyBr_4$.[25,26]

In the present paper, we report a combined MI-IR and computational study of the $MDyX_4$ complexes. The computations have been performed for all possible variations with M = Li, Na, K, Rb, Cs and X = F, Cl, Br, and I. The main goal of the present work is to predict the thermodynamic behavior of these molecules, particularly in the high-temperature vapors of metal−halide discharge lamps. We have also investigated the ionization energies of the complexes and the dissociation processes of the cations since ionization and dissociation might be of relevance at the high temperatures encountered in the lamps. Our experimental infrared spectroscopic study includes three complexes, $NaDyBr_4$, $CsDyBr_4$, and $CsDyI_4$. To overcome the difficulties of possible low concentration and broad absorption bands in the IR spectra of the vapors, we have applied the matrix-isolation technique assisted by the computation of the thermodynamic and vibrational properties of the possible vapor-phase species. Besides focusing on an unambiguous assignment of the molecular symmetry, particular attention was paid to the experimental confirmation of the presence of certain minor components in the vapor.

COMPUTATIONAL AND EXPERIMENTAL DETAILS

Computational Methodology. Considering the large number of species to be calculated (about 80), it was important to use a computational method/basis set combination that is fast enough and, at the same time, gives reliable results. Therefore, first we tested different computational methods; several density functional (B3LYP,[27,28] B3PW91,[27,29] and mPW1PW91[30]) and the MP2 methods.[31] After different trials, eventually we used the following basis sets: the dysprosium atom was described by a "large-core" (LC) ECP involving 55 electrons ($[Kr]4d^{10}4f^9$) and an associated basis set of the (7s6p5d)/[5s4p3d] type augmented with two f polarization functions from Dolg (α_f = 1.158, α_f = 0.416).[32−34] For the light atoms the cc-pVTZ-type all-electron bases (Li and F,[35] Na,[36] Cl[37]) were used, and for the remaining atoms pseudopotentials from the Stuttgart group with associated basis sets: for Br and I SDB-cc-pVTZ-type[38,39] and for K, Rb, Cs small-core Stuttgart MDF type ECPs,[40] in the case of Rb and Cs the g functions were removed from the basis.

The choice of those particular basis sets was based on the following considerations: according to our previous experience with $DyBr_3$[41] and $NaDyBr_4$,[25,26] the use of small-core (SC) bases, in which the electrons of the $(n - 1)$ shell are included in the valence basis set, causes serious difficulties for the calculation. This is due to the fact that the many different possibilities of the 4f electron configuration unrealistically increase the computational time. We compared the results of small- and large-core calculations (considering the Dy basis) for different methods and we found that the Dy−Br bond length is only about 0.03 Å longer from the mPW1PW91 LC calculation than the estimated experimental bond length,[41,42] or the bond length from the MP2 SC calculation. Therefore, we decided to use the LC bases for Dy. As for the description of the larger alkali atoms (K, Rb, Cs), on the other hand, it was essential to use SC basis sets, because after the ionization of an alkali atom the original valence shell becomes empty and the $(n - 1)$ shell becomes the valence shell, it would be a mistake to leave that out. The comparison of the large- and small-core (alkali atoms) calculations verifies this; using the same method the difference in the M−Br bond lengths is usually around 0.1 Å! For the smaller atoms the cc-pVTZ basis sets were used that provide a balanced description for all molecules calculated.

The mPW1PW91 density functional method was applied, which uses the modified Perdew−Wang exchange functional with a gradient-corrected Perdew−Wang 91 correlation functional.[30] All geometry, frequency, and BSSE calculations were performed with the Gaussian 98 and 03 program packages.[43,44] Ionization potentials calculated for $NaDyBr_4$ with the mPW1PW91 method and the chosen basis set agree very well with the experimental results. However, this level of theory somewhat underestimates the experimental dissociation enthalpy and entropy data for the $MDyX_4$ species (M = Na, Cs and X = Br, I) by, on average, 30 kJ·mol^{-1} and 10−15 J·mol^{-1}·K^{-1}, respectively.[2,8,9,45]

Since our computations involved ions as well as radicals, we had to check whether the LC ECPs (that treat the 4f subshell in the core) can describe these systems properly. Therefore, we carried out mPW1PW91 test calculations with a small core ECP and its associated basis set[46,47] using the Gaussian 09 program package.[48]

Samples. Ultrapure $DyBr_3$(s) and DyI_3(s) samples were provided by Philips Lighting B.V., The Netherlands and NaBr(s), CsBr(s) and CsI(s) by NRG, Petten, The Netherlands. The purity of the samples was confirmed by measuring their X-ray patterns. In order to prevent excessive evaporation of the alkali halide from the furnace before complex formation could occur, the experiments were performed with ternary systems which were synthesized prior to the experiments. The stoichiometries of the samples were selected from their phase diagrams and correspond to compositions where new ternary systems are formed. For the NaBr−$DyBr_3$ mixture this occurs at a mole ratio ($NaBr/DyBr_3$) of 3:1.[49] The CsX−DyX_3 (X = Br, I) mixtures were synthesized with a mole ratio (CsX/DyX_3) of 5:2,[50] while in addition in case of X = I, also a 4:3 (CsI/DyI_3) mixture was prepared.[50] This latter mixture allows us to investigate the influence of the starting composition on the evaporation behavior. The preparative procedure generally consisted of mixing the finely powdered binary compounds followed by sealing the mixture in an evacuated quartz ampule. Prior to the filling procedure, the quartz ampules were outgassed at 1200 K for 12 h under 5% H_2/95% Ar atmosphere. The closed vessel with the mixture was heated for 128 h at a temperature below the melting point of the mixture or for 1 h with the mixture in the molten state. The X-ray patterns of the materials synthesized by these two methods did not differ. For the specific samples used in this study we used 128 h at

dx.doi.org/10.1021/ic202009v | Inorg. Chem. 2012, 51, 543−556

925 K in case of the NaBr−$DyBr_3$ mixture, 128 h at 850 K in case of the CsBr−$DyBr_3$ mixture, and 1 h at 1150 K in case of the CsI−DyI_3 mixtures. The resulting powders were reground before use in the matrix-isolation depositions. All sample handlings of the extremely oxygen and moisture sensitive compounds were carried out in an argon-filled glovebox at NRG.

Matrix-Isolation Infrared Spectroscopy. The apparatus for matrix-isolation experiments consists of a Displex DE 202 cryotip (Air Products and Chemicals, Allentown, PA), which can be rotated in a homemade stainless steel vacuum shroud. A homemade stainless steel high-temperature resistance furnace is mounted to the vacuum shroud. A copper block with a thin polished layer of nickel served as deposition surface. The temperature of the deposition window was usually in the range of 15−30 K during formation of the matrices; its temperature being monitored by a chromel−(gold+0.3% Fe) thermocouple. An oscillating quartz crystal microbalance is attached to the cryogenic surface[51] to sample the molecular beam effusing from the sample cell. High-purity xenon 4.5 or krypton 4.5 (99.995%, Air Products Nederland B. V., Waddinxveen, The Netherlands) were employed as the isolating gas without further purification. The matrix gas was generally deposited at a rate of 0.4 - 0.7 mL/min, measured by a calibrated gas-flow meter (model 5860E/-1AB3B, Inacom Instruments B. V., Veenendaal, The Netherlands). Contact of the moisture- and oxygen-sensitive samples with ambient atmosphere during filling of the equipment could be avoided by using the glass-cartridge method from Klotzbücher,[52] adapted for high-temperature evaporation conditions. The samples were put into narrow graphite tubes, which were surrounded by a quartz tube, sealed under high vacuum conditions. Prior to the filling of the cells in an argon-filled glovebox, both the graphite inner tube and the quartz outer tube were outgassed for 12 h under 5% H_2/95% Ar atmosphere. After reaching a vacuum of 10^{-5} mbar in the matrix-isolation equipment, the top of the quartz tube was opened by a hammer mounted on the heat shield.

The evaporation of the MX−DyX_3 (M = Na, Cs; X = Br, I) samples was performed in the temperature range 900−1000 K; deposition times varied between 45−180 min. The furnace temperature was measured by a K-type thermocouple (Thermocoax FKI 10/10) positioned in the stainless steel furnace body near the sample. The IR spectra of matrix-isolated species were recorded in reflection mode with a Bomem DA3.02 Fourier-transform spectrometer equipped with a Bomem APG 7400D mirror bench. A homemade vacuum flange connected the cryostat with the interferometer. Measurements were performed through a wedged polyethylene outer window in the cryostat. Resolution was 0.5 cm^{-1} or better; 256 scans were coadded. Our study covered the spectral region from 20 up to 375 cm^{-1}. Usually this spectral window was covered by applying two different optical combinations. For the 20−100 cm^{-1} range a mercury light source with a 25 μm Mylar beamsplitter was used, while the 75−375 cm^{-1} region was recorded by using a globar light source in combination with a 6 μm Mylar beamsplitter. A helium-cooled germanium bolometer operating at 4.2 K was used for detection in both cases. Several of the spectra shown in the paper are a combination of two spectra obtained this way.

For the CsI−DyI_3 measurements sometimes a mercury light source with a 12 μm Mylar beamsplitter was used. This optical combination enabled us to measure all the signals of the evaporated species in one measurement (from ~35 up to 240 cm^{-1}), and was used only after it was established that these evaporations and the subsequent annealing sessions did not result in signals above 240 cm^{-1}.

The spectra were baseline corrected and the water rotation bands resulting from residual molecules in the evacuated spectrometer were subtracted.

RESULTS AND DISCUSSION

Computation of Neutral Complexes. Geometrical parameters, vibrational frequencies, and energies of all $MDyX_4$ (M = alkali metal, X = halogen) mixed halides are given in the Supporting Information. They follow the trends observed earlier in some of these and also other mixed alkali-metal/lanthanide complexes.[22−25] From the three isomers shown in Figure 1, only the bidentate and tridentate forms are always real minima on the potential energy surface (PES) and they have relevance in real systems. The monodentate structure has been found to be a high-lying local minimum on the potential energy surface when X = F and it is a first-order saddle-point on the various possible paths between bidentate and tridentate minima for the other halides. The present computations showed the same features for the $MDyX_4$ compounds.

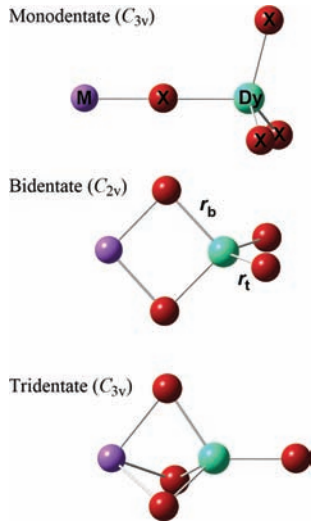

Figure 1. Three possible isomers of $MDyX_4$ (M = alkali metal, X = halogen) molecules.

Our earlier studies also showed that the relative energies of the bi- and tridentate structures depend on the temperature.[22−25] While at zero Kelvin the complexes of lighter halogens and alkali metals prefer the C_{2v} bidentate structure, the heavier ones prefer the C_{3v} tridentate arrangement. Thermodynamic calculations on selected structures showed that the contribution of the entropy at experimentally meaningful high temperatures (>800 K) acts in favor of the bidentate structure.[24,25]

Our present study provides a more detailed picture about the effect of entropy on the relative stability of $MDyX_4$ compounds. Figure 2a refers to 0 K, where the relative energies predict the higher stability of the tridentate form for all complexes, except for the fluorides and all lithium halides. The relative energy curves show a gradual decrease with increasing atomic masses of M and X. The energy data of the fluorides differ considerably from those of the heavier halides, and so do the data of Li and, to a lesser extent, Na, from those of the heavier alkali metals. On the other hand, the relative energies of the K, Rb and Cs chlorides, bromides and iodides are quite close to each other with marginal differences between the K−Rb−Cs analogues.

Figure 2b demonstrates the Gibbs free energy differences of the two structure types at 1000 K. At this temperature, the bidentate structures become more stable for all the halides. The gradually decreasing slope of the potential energy (cf., Figure 2a) can still be recognized in the ΔG^{1000K} values of the fluorides, while the other complexes show a minimum-type curve. The enthalpy differences show the same decreasing trend as the energies; but the entropy part ($-T\Delta S$) increases nonmonotonically with temperature (except for the fluoride), resulting in a minimum-type trend ΔG^{1000K} for the complexes of larger alkali metals.

dx.doi.org/10.1021/ic202009v | Inorg. Chem. 2012, 51, 543−556

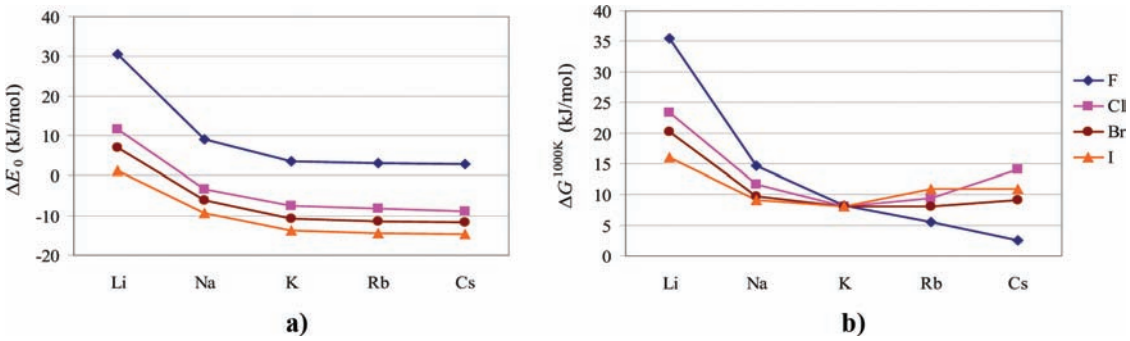

Figure 2. Relative stability of bidentate vs tridentate structures in terms of (a) zero-point energy ($\Delta E_0 = E_{0,\text{tridentate}} - E_{0,\text{bidentate}}$, kJ/mol) and (b) Gibbs free energy at 1000 K ($\Delta G^{1000K} = G_{\text{tridentate}} - G_{\text{bidentate}}$, kJ/mol). All relevant data are given in the Supporting Information.

The stability of the complexes can be assessed from the dissociation energies. In Figure 3, we compiled the computed Gibbs free energies of dissociation at 1000 K for three dissociation routes. Among them the one to neutral MX + DyX_3 fragments (Figure 3a) is the most favorable at 1000 K, the Gibbs free energy change of the reaction being below 150 kJ/mol for all species. The ΔG values cover a rather narrow (100 kJ/mol) range and show a slightly increasing trend with the change of the alkali metal. The only exceptions are the fluorides that give a maximum-type ΔG curve.

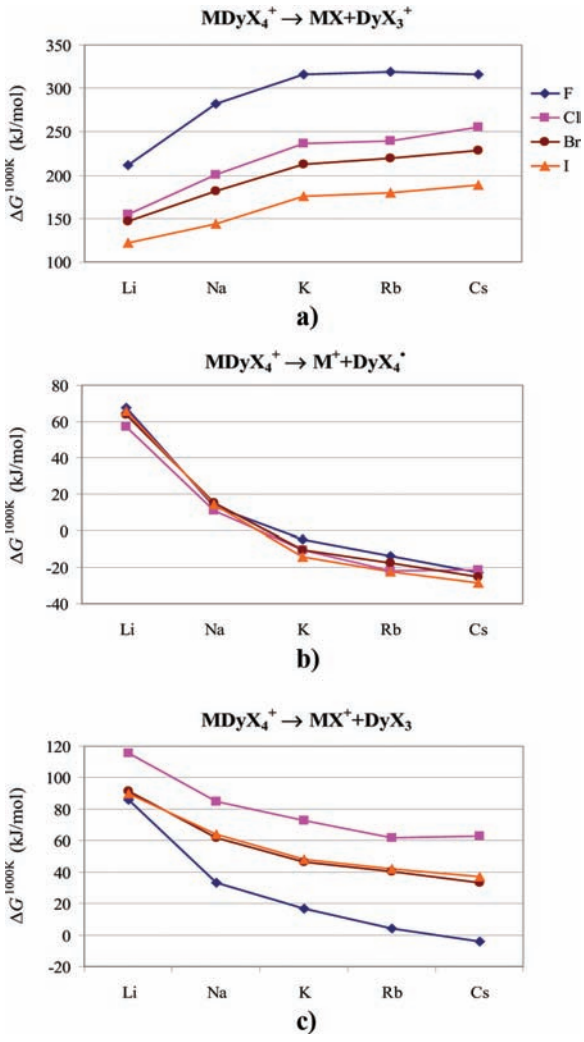

Figure 3. Computed Gibbs free energies of dissociation at 1000 K (kJ/mol) of the neutral complexes to (a) neutral fragments, (b) ionic fragments, and (c) radical fragments. Solid lines represent the trends in the bidentate, while dotted lines the trends in the tridentate structures.

Comparison with our previous studies of $MLaX_4$ complexes[23,24] reveals that the $MDyX_4$ complexes are slightly more stable than their $MLaX_4$ analogues. This feature can primarily be attributed to the shorter/stronger Ln−X bonds in the Dy complexes (during the dissociation one bond is breaking) as a result of the lanthanide contraction.

The dissociations to ionic $M^+ + DyX_4^-$ (Figure 3b) and radical $M^\bullet + DyX_4^\bullet$ (Figure 3c) fragments are less advantageous because of the lack of stabilization of these fragments in the gaseous phase. The range covered by the ΔG values is wider (250−600 kJ/mol) than for dissociation to neutral fragments (cf., Figure 3a). A considerable decreasing trend with increasing atomic mass of the alkali metal can be observed in case of the ionic fragments, in agreement with the expected trend for attractive electrostatic interactions between the alkali metals and the halogens. Obviously, in these systems the main part of dissociation is the separation of the, already in the molecule, strongly ionic fragments.

Differing from the previous two processes, the Gibbs free energy of dissociation to the radical fragments shows a minimum-type curve (Figure 3c). The radical fragments are formed by charge transfer from the DyX_4 moiety to the positively charged strongly electron deficient alkali atom. The natural charges determined in previous studies for $MLaX_4$ complexes[23,24] indicate a smaller positive charge for Na compared to the other alkali metals. The similar curves indicate that the energy of dissociation is mostly determined by the $DyX_4^- \rightarrow M^+$ charge transfer.

Computation of Cationic Complexes. Under the operating conditions of metal halide lamps, some ionization may take place. This prompted us to compute the ionization potentials and some other properties of the cationic $MDyX_4^+$ complexes. The adiabatic ionization potentials are given in the Supporting Information and are shown in Figure 4a. Both the magnitudes and trends compare well with those of the respective MX halides presented in Figure 4b. (Note that we chose to compute the MX ionization potentials as well since the experimental literature data[53] show a strongly scattering pattern.) The slopes of the $MDyX_4$ ionization potentials are somewhat flatter than those of MX, reflecting a buffer effect of the larger number of halogens in the complexes.

The Mulliken atomic charges that have been evaluated for the four outermost cases ($LiDyF_4$, $CsDyF_4$, $LiDyI_4$, and $CsDyI_4$), showed that at ionization of the $MDyX_4$ complexes the electron

dx.doi.org/10.1021/ic202009v | Inorg. Chem. 2012, 51, 543−556

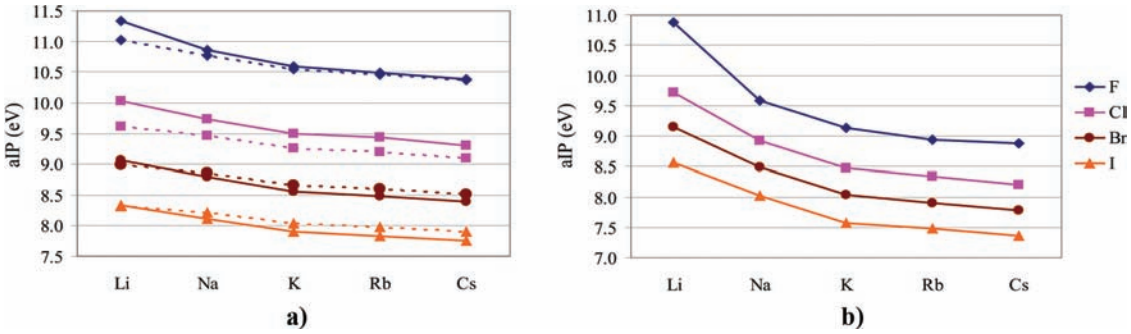

Figure 4. Computed adiabatic ionization potentials (eV) of (a) $MDyX_4$ (solid line, bidentate; dotted line, tridentate) and (b) MX.

leaves mainly from the terminal halogens. The atomic charges of the two terminal halogens in the bidentate structures decrease by 0.6−0.7 e upon ionization; the rest leaves mainly from Dy and M. The charge of the bridging halogens decreases only slightly. In the tridentate structures, the loss of charge from the single terminal halogen makes the formed tridentate ions unstable, they are first-order saddle points on the PES. Relaxations of these tridentate cationic structures led to the bidentate cationic structures in all cases. There is no indication that the situation would be different for the intermediate $MDyX_4$ species.

Structurally, the Dy−X_t bonds are longer in the bidentate cations than in the neutral complexes and their X_t−Dy−X_t bond angles decrease to about 60° from the 120° in the neutral complexes. Analogous features have been observed in theoretical studies of LnX_3^+ ions.[54,55] As a result of the decreased terminal bond angle the two X_t atoms get very close to each other; their distance is between the sums of the respective covalent and van der Waals radii of the halogens (the fluorides, chlorides and bromides closer to the sum of the covalent radii). This short distance implies a bonding interaction between the two terminal halogens that is supported by the presence of bond critical points between the two halogens as shown in Figure 5

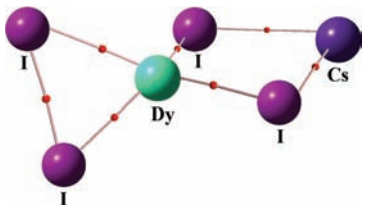

Figure 5. Bond critical points (small red balls) in the $CsDyI_4^+$ cation.

based on Bader analysis.[56,57] We observed analogous features upon formation of the $DyX_4^•$ radicals from the DyX_4^- anions.

We note that the legitimacy of the LC ECP of Dy (assuming a $4f^9$ configuration and constraining the 4f electrons to the core) was confirmed by test calculations applying the Cundari small-core ECP that leaves the 4f orbitals in the valence shell. These calculations were carried out for the DyX_4^- and $DyX_4^•$ species with X = F and I, and resulted in a $4f^9$ configuration on Dy in both cases. This configuration, characteristic for Dy(III), is expected for DyX_4^-. In $DyX_4^•$, which can be derived from DyX_4^- by removing one electron, it is likely that the electron leaves from the halogens because the fourth IP of Dy is very high (3990 kJ/mol compared to the third IP of 2200 kJ/mol).[58]

The computed Gibbs free energies of dissociation at 1000 K (Figure 6) indicate that the $MDyX_4^+$ cations have a much lower

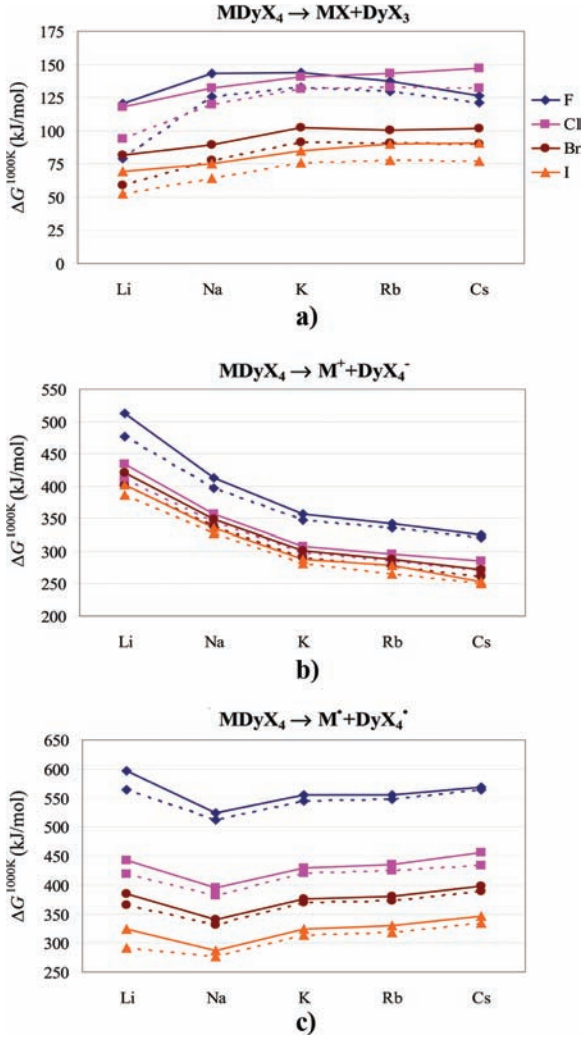

Figure 6. Gibbs free energies (in kJ/mol) of dissociation of the $MDyX_4^+$ cations to (a) MX + DyX_3^+, (b) M^+ + $DyX_4^•$, and (c) MX^+ + DyX_3 at 1000 K.

stability than their neutral $MDyX_4$ analogues. The curves have similar character to the ones of the respective dissociations from $MDyX_4$ to neutral and ionic fragments (cf. Figure 3). We note the negative $\Delta G^{1000\ K}$ values of $MDyX_4^+ \rightarrow M^+ + DX_4^•$ reactions for M = K, Rb, Cs (Figure 6b) and for $CsDyF_4^+ \rightarrow CsF^+ + DyF_3$, (Figure 6c), indicating that these cationic complexes are probably not stable at such high temperatures.

Figure 7 demonstrates the computed dissociation energies of the bidentate isomers of $LiDyF_4$ and $CsDyI_4$ indicating the

dx.doi.org/10.1021/ic202009v | Inorg. Chem. 2012, 51, 543−556

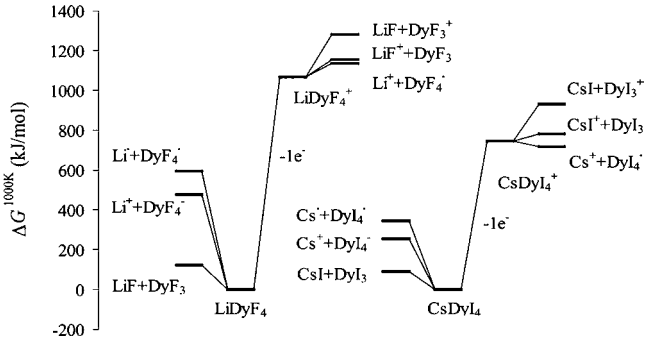

Figure 7. Computed Gibbs free energies of dissociation (at 1000 K) of the bidentate isomer of neutral and cationic $LiDyF_4$ and $CsDyI_4$.

relationship between the various dissociation paths as well as between the light and heavy $MDyX_4$ complexes.

Modeling of the Isomerization Equilibrium for $NaDyBr_4$, $CsDyBr_4$, and $CsDyI_4$. The computed energy data (ΔE and dissociation energies) and selected molecular parameters of the experimentally investigated compounds are given in Table 1 for their chemically relevant bidentate and tridentate isomers.

Table 1. Calculated Energies and Geometrical Parameters of the $CsDyBr_4$, $CsDyI_4$, and $NaDyBr_4$ Complexes[a]

	$CsDyX_4$		
	X = Br	X = I	$NaDyBr_4$
	bidentate		
D_0	215.8	198.4	211.2
Dy–X_t	2.640	2.863	2.630
Dy–X_b	2.740	2.969	2.765
M–X_b	3.401	3.637	2.744
X_t–Dy–X_t	115.6	115.0	115.7
X_t–Dy–X_b	110.7	110.2	111.3
X_b–Dy–X_b	97.1	100.2	93.9
M–X_b–Dy	94.3	91.1	85.6
	tridentate		
D_0	225.5	210.4	215.5
Dy–X_t	2.643	2.864	2.639
Dy–X_b	2.703	2.930	2.710
M–X_b	3.576	3.808	2.929
X_t–Dy–X_b	119.2	117.9	122.5
X_b–Dy–X_b	98.3	99.8	93.8
M–X_b–Dy	77.9	75.1	71.3
	Bi → Tri[b]		
ΔE_e	0.2		3.5
ΔE_0	0.2		3.4
	Tri → Bi[b]		
ΔE_e	12.2		9.9
ΔE_0	12.0		9.6

[a]The dissociation energies to neutral fragments (D_0, kJ/mol) have been corrected for BSSE and zero-point vibrational energy. In the geometrical parameters (Å, deg) the terminal and bridging halogens are indicated by the corresponding abbreviations. [b]Energy barriers for the interconversion between the two structures (kJ/mol). ΔE_e means the electron energy differences, while ΔE_0 includes zero-point vibrational energy correction.

The small energy differences between the bidentate and tridentate structures suggest that both isomers can be expected to be present in the vapor. From the ΔG values between the isomers we derived the equilibrium constants of the bidentate ↔ tridentate isomerization processes by evaluating $-RT \ln K_p = \Delta H^\circ(T) - T\Delta S^\circ(T)$. The derived relative amounts of the bi- and tridentate structures in the temperature range T = 0–3000 K are presented in Figure 8.

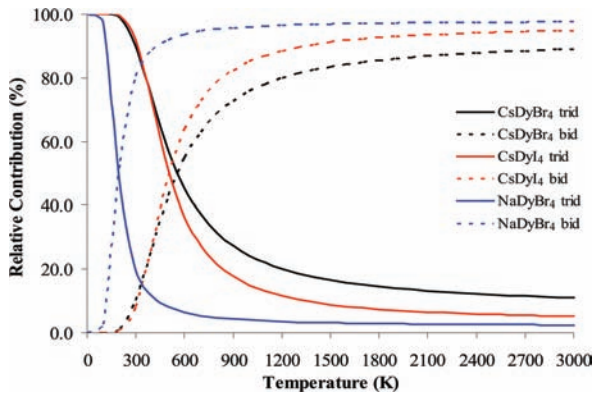

Figure 8. Relative amounts of the bi- and tridentate structures in the temperature range T = 0–3000 K on the basis of the computed Gibbs free energy differences.

According to the relative stabilities at 0 K (vide supra) these complexes are characterized by a negative enthalpy change (ΔH°) for the bidentate → tridentate isomerization process. The entropy change of the isomerization (ΔS°), as determined by the change in symmetry upon going from bidentate to tridentate, is negative leading, however, to a positive entropy term ($-T\Delta S^\circ$). Altogether, all three complexes prefer the tridentate isomer at low temperatures, whereas the positive entropy term ($-T\Delta S^\circ$) results in an increase of the relative amount of the bidentate structure with increasing temperature. At temperatures, where the complexes exhibit sufficiently high vapor pressures for matrix isolation experiments (T > 900K), the bidentate structure is predicted to dominate over the tridentate isomer. For the $NaDyBr_4$ complex, the anticipated amount of the tridentate structure is expected not to exceed 4%. It should be noted, however, that the accuracy of the curves in the low-temperature range (that is between 200 and 1000 K with the considerably changing concentrations) depends strongly on the accuracy of the computed energy differences that, however, is almost impossible to estimate considering the inherent uncertainty of the effect of the applied computational methods and basis sets. It is worth mentioning that the uncertainty of the computational level of theory also influences the amount of different isomers at the high-temperature range (where the $-T\Delta S^\circ$ term dominates), but there this is mostly due to their influence on the computed low-wavenumber fundamentals.

In the matrix-isolation experiments (vide infra) an additional effect has to be taken into account: that of the matrix (noble gas) environment surrounding the $MDyX_4$ species. Although it is assumed that in these experiments the high temperature situation is frozen out on the cold window, there are studies indicating that changing the matrix host results in different structural isomers.[59,60] First, for selected individual complexes ($NaDyBr_4$, $CsDyBr_4$, and $CsDyI_4$), we investigated the energy profile of the interconversion of the bidentate to the tridentate structure on the PES with the relaxed scan method. Previously, we reported the gas-phase activation energy barrier of the bidentate → tridentate conversion of $NaDyBr_4$ obtained at a similar (B3PW91/TZP) computational level to be 3.2 kJ/mol.[25] According to our present

dx.doi.org/10.1021/ic202009v | Inorg. Chem. 2012, 51, 543–556

computations, the barrier for the bidentate → tridentate interconversion of $CsDyBr_4$ is considerably smaller (0.2 kJ/mol), while $CsDyI_4$ has no barrier at all, just a wide flat range in the spatial vicinity of the bidentate structure even though this structure lies 17.4 kJ/mol higher than the tridentate one. In contrast, the energy barrier for the opposite interconversion (tridentate → bidentate) was computed to be 8.4 kJ/mol for $NaDyBr_4$,[25] while 12.2 kJ/mol for $CsDyBr_4$ (for $CsDyI_4$ there is no barrier). These characteristics of the PES can make the equilibrium sensitive to the weak interactions of the heavier rare gases with the species present in the vapor.

In a second step, we calculated the effect of the rare gas matrix on the relative stabilities of the bidentate and tridentate structures. According to the Onsager model,[61,62] the energy difference between the isomers of $NaDyBr_4$ and $CsDyBr_4$ becomes smaller in the matrix. The preferences for the tridentate structure by 6.2 and 11.6 kJ/mol (in electronic energy) in the gas-phase decreased to 0.2 and 5.0 kJ/mol in a Xe matrix, respectively. In the case of $CsDyI_4$ we found that the order of relative stability is reversed. While in vacuum the bidentate isomer is less stable than the tridentate by 17.4 kJ/mol, in the matrix the bidentate becomes the more stable structure with 3.1 kJ/mol.

Computed IR spectra of $NaDyBr_4$, $CsDyBr_4$, and $CsDyI_4$. Beyond the structural and energetic properties, the computations provide important vibrational data, which can be used to assist the interpretation of experimental vibrational spectra. The computations are particularly advantageous for predicting small differences between structural isomers with similar frequencies, where the experimental information alone is insufficient to distinguish between them. Our previous theoretical studies on $MLnX_4$ complexes indicated the potential of IR spectroscopy in distinguishing between the bidentate and tridentate structures, while the computed Raman spectra of the two isomers showed no characteristic differences.[23,24]

The computed infrared spectra of the two stable isomers of $CsDyBr_4$, $CsDyI_4$, and $NaDyBr_4$, are shown in Figure 9 and the data are tabulated in Tables 2, 3, and 4, respectively. The spectra of the same isomers in the three compounds are very similar; the only differences are due to the differences in the atomic weights in pairs of compounds (Na vs Cs and Br vs I).

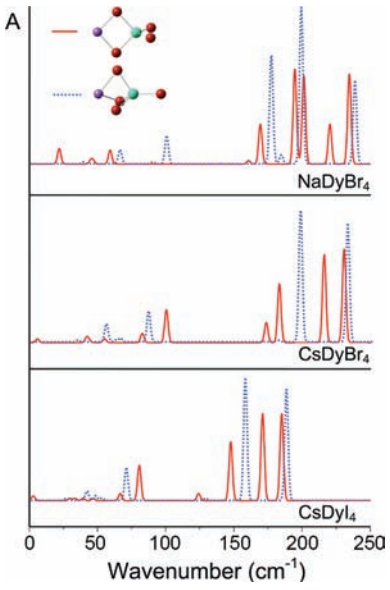

Figure 9. Calculated IR spectra of the bi- (red/solid line) and tridentate (blue/dotted line) structures of $NaDyBr_4$, $CsDyBr_4$, and $CsDyI_4$.

Figure 9 shows significant differences between the infrared spectra of the bidentate and tridentate structures for each species. The tridentate structure has fewer vibrational bands compared to the bidentate because of the degeneracy in the C_{3v} point group. The most characteristic difference between the spectra of the two structures of the $CsDyX_4$ species appears in the region of the Dy−X stretching vibrations. Therefore, for these complexes this region will be of the greatest value in the structural assessment on the basis of the experimental infrared spectra. The computed spectra of the $CsDyX_4$ bidentate structures consist of three strong bands in the Dy−X stretching region: ν_1 (A_1 symmetric Dy−X_t terminal stretch), ν_7 (B_2 antisymmetric Dy−X_b ring stretch) and ν_{10} (B_1 antisymmetric Dy−X_t stretch). Beside these three strong bands a weak one is predicted in this spectral region representing the symmetric Dy−X_b stretch, ν_2. In contrast, the calculated infrared spectrum of the tridentate structure only features two bands in the region of Dy−X stretching fundamentals: ν_1 (A_1 Dy−X_t stretch) and ν_5 (E antisymmetric Dy−X_b stretch). The symmetric Dy−X_b stretch ν_2 of the tridentate isomer has hardly any computed IR intensity, being about 15% of the already low intensity of the corresponding fundamental of the bidentate structure.

The Cs−X stretching fundamentals and the deformation modes are all of weak IR intensity with wavenumbers below 100 cm^{-1}, a region experimentally difficult to access. Moreover, the computed frequencies of the two structures differ only slightly (~10 cm^{-1}) and this small difference is insufficient to distinguish between the two structures, unless both appear in the spectrum.

The IR spectra of the $NaDyBr_4$ species differ from those of the cesium complexes in the position of the Na−Br stretching bands, appearing in the region of the Dy−X stretching vibrations. As can be seen in Figure 9, a total of five absorptions can be expected in this region for the bidentate $NaDyBr_4$, three of them strong and two having medium intensity. The calculated spectrum for the tridentate isomer consists only of three intense bands. Similarly to the cesium complexes, the low-wavenumber region is less characteristic.

Interpretation of the MI-IR Spectra of $NaDyBr_4$, $CsDyBr_4$, and $CsDyI_4$ in Kr and Xe Matrices. Representative spectra of the vapors of the mixtures CsBr−$DyBr_3$, CsI−DyI_3 (both 5:2 molar ratio), and NaBr−$DyBr_3$ (3:1 molar ratio) trapped in krypton and xenon matrices are shown in Figures 10, 11, and 12, respectively.

According to mass spectroscopic studies on related ternary systems (see e.g. refs 2, 5), the composition of their vapor phase is rather complex: in equilibrium vapors the LnX_3, MX and M_2X_2 species can be expected in considerable amounts in addition to the $MLnX_4$ complexes. They give absorption bands near the expected absorptions of $MLnX_4$. Therefore, prior to the discussion of the spectra obtained on the title complexes, the spectral characteristics of the binary parent compounds should be elucidated.

Recently, we performed extensive investigations on CsX[63] and DyX_3 (X = Br,[41] I[64]) using the same experimental setup as in the present study. The $DyBr_3$ results were used to assign the low intensity splitted bands in the matrix-IR spectra of the NaBr−$DyBr_3$ mixture with maxima at 238.2/244.7 cm^{-1} (Kr) and at 229.1/232.0/233.9 cm^{-1} (Xe) to the antisymmetric stretch fundamental ν_3 of monomeric $DyBr_3$. In the matrix-IR spectrum of the isolated vapor of the CsBr−$DyBr_3$ mixture a similar assignment was made for the bands with maxima at 234.3/238.1 cm^{-1} (Kr) and at 228.7/231.9 cm^{-1} (Xe). The ν_3

dx.doi.org/10.1021/ic202009v | Inorg. Chem. 2012, 51, 543−556

Table 2. Experimental and Calculated Vibrational Frequencies ν_i (cm^{-1}) of the Bidentate and Tridentate Isomers of $CsDyBr_4$ (g)

	assignment			frequency	frequency, experimental		
	symmetry	ν_i	character[b]	calculated[a]	krypton	xenon	matrix shift
bidentate	A_1	1	ν_sDy−Br_t	216 (48)	203.6	198.4	5.2
		2	ν_sDy−Br_b	173 (11)	176.8	171.8	5.0
		3	ν_sCs−Br	100 (18)	86.6	83.2	3.4
		4	βDy−Br_b	62 (<1)			
		5	sciDy-Br_t	42 (3)			
	A_2	6	twDy-Br_t	40 (0)			
	B_1	10	ν_{as}Dy−Br_t	230 (51)	220.7	214.3	6.4
		11	ring puckering	55 (2)			
		12	wCs	5 (2)			
	B_2	7	ν_{as}Dy−Br_b	183 (32)	198.7	193.5	5.2
		8	ν_{as}Cs−Br	82 (5)			
		9	wDy-Br_t	44 (1)			
tridentate	A_1	1	νDy−Br_t	232 (65)	217.8	~214	3.8
		2	ν_sDy−Br_b	181 (1)			
		3	ν_sCs−Br_b	86 (17)			
		4	δ_sDy−Br_b	65 (2)			
	E	5	ν_{as}Dy−Br_b	197 (71)	206.7	203.4	3.3
		6	δ_{as}Dy−Br_b	61 (<1)			
		7	ν_{as}Cs−Br_b	55 (10)			
		8	βCs−Dy−Br_t	34 (<1)			

[a]IR intensities ($km \cdot mol^{-1}$) are given in parentheses. [b]The symbols or abbreviations ν, β, δ, sci, tw, w, s, as, t, b mean stretch, in-plane bend, deformation, scissoring, twist, wag, symmetric, asymmetric, terminal, and bridging, respectively.

Table 3. Experimental and Calculated Vibrational Frequencies ν_i (cm^{-1}) of the Bidentate and Tridentate Isomers of $CsDyI_4$ (g)

	assignment			frequency	frequency, experimental		
	symmetry	ν_i	character[b]	calculated[a]	krypton	xenon	matrix shift
bidentate	A_1	1	ν_sDy−I_t	171 (37)	165.8	160.9	4.9
		2	ν_sDy−I_b	124 (3)	132.1	125.8	6.3
		3	ν_sCs−I	81 (15)	73.0	68.6	4.4
		4	βDy−I_b	47 (<1)			
		5	sciDy-I_t	30 (1)			
	A_2	6	twDy-I_t	28 (0)			
	B_1	10	ν_{as}Dy−I_t	185 (37)	183.1	175.2	7.9
		11	ring puckering	39 (1)			
		12	wCs	3 (2)			
	B_2	7	ν_{as}Dy−I_b	148 (25)	158.9	153.8	5.1
		8	ν_{as}Cs−I	67 (3)			
		9	wDy-I_t	33 (<1)			
tridentate	A_1	1	νDy−I_t	188 (47)	~179	~175	4.0
		2	ν_sDy−I_b	128 (<1)			
		3	ν_sCs−I_b	70 (14)			
		4	δ_sDy−I_b	52 (1)			
	E	5	ν_{as}Dy−I_b	157 (53)	~170	166.8	3.2
		6	δ_{as}Dy−I_b	48 (1)			
		7	ν_{as}Cs−I_b	41 (5)			
		8	βCs−Dy−I_t	26 (1)			

[a]IR intensities ($km \cdot mol^{-1}$) are given in parentheses. [b]The symbols or abbreviations ν, β, δ, sci, tw, w, s, as, t, b mean stretch, in-plane bend, deformation, scissoring, twist, wag, symmetric, asymmetric, terminal, and bridging, respectively.

signal of DyI_3 in the matrix isolation spectra of CsI−DyI_3 mixtures is observed as a doublet at 188.8/194.1 cm^{-1} in xenon or in the form of an even more complex signal with maxima at 190.1/192.5/197.8 cm^{-1} in krypton. We note that in the spectra of pure $DyBr_3$ and DyI_3 we obtained signals with lower complexity at wavenumbers near the peaks of the present splitted bands. The splitting of the bands in the present spectra might be attributed to a site effect of the matrix containing many different species. Annealing of the matrices seriously reduces this influence and the resulting DyX_3 ν_3 signal resembles the spectrum of the pure compound (vide infra, Figure 14).

In agreement with the previously studied matrix-IR spectra of CsBr and CsI,[63] the stretching fundamental of CsBr shows the bromine isotopic splitting and as a consequence appears as a doublet at 125.6/126.5 (Kr) or 119.3/120.1 cm^{-1} (Xe). The CsI fundamental gives a strong sharp peak at 102.9 cm^{-1} (Kr) or 96.1 cm^{-1} (Xe). The wide bands on the low-wavenumber

dx.doi.org/10.1021/ic202009v | Inorg. Chem. 2012, 51, 543−556

Table 4. Experimental and Calculated Vibrational Frequencies ν_i (cm^{-1}) of the Bidentate and Tridentate Isomers of $NaDyBr_4$ (g)

	assignment			frequency	frequency, experimental		
	symmetry	ν_i	character[b]	calculated[a]	krypton	xenon	matrix shift
bidentate	A_1	1	ν_sDy−Br_t	220 (23)	205.2	195.8	9.4
		2	ν_sNa−Br_b	195 (55)	188.6	181.6	7.0
		3	ν_sDy−Br_b	169 (23)	176.0	170.1	5.9
		4	βDy−Br_b	83 (<1)			
		5	sciDy-Br_t	46 (2)			
	A_2	6	twDy-Br	38 (0)			
	B_1	10	ν_{as}Dy−Br_t	235 (52)	228.6	222.1	6.5
		11	ring puckering	59 (8)			
		12	wNa	21 (9)			
	B_2	7	ν_{as}Na−Br_b	201 (51)	199.8/197.3	189.2	8.1
		8	ν_{as}Dy−Br_b	160 (2)	159.3		
		9	wDy-Br_t	44 (2)			
tridentate	A_1	1	νDy−Br_t	238 (47)			
		2	ν_sDy−Br_b	184 (5)			
		3	ν_sNa−Br_b	177 (61)			
		4	δ_sDy−Br_b	90 (1)			
	E	5	ν_{as}Dy−Br_b	199 (88)			
		6	ν_{as}Na−Br_b	100 (16)			
		7	δ_{as}Dy−Br_b	66 (8)			
		8	βNa−Dy−Br_t	39 (1)			

[a]IR intensities ($km \cdot mol^{-1}$) are given in parentheses. [b]The symbols or abbreviations ν, β, δ, sci, tw, w, s, as, t, b mean stretch, in-plane bend, deformation, scissoring, twist, wag, symmetric, asymmetric, terminal, and bridging, respectively.

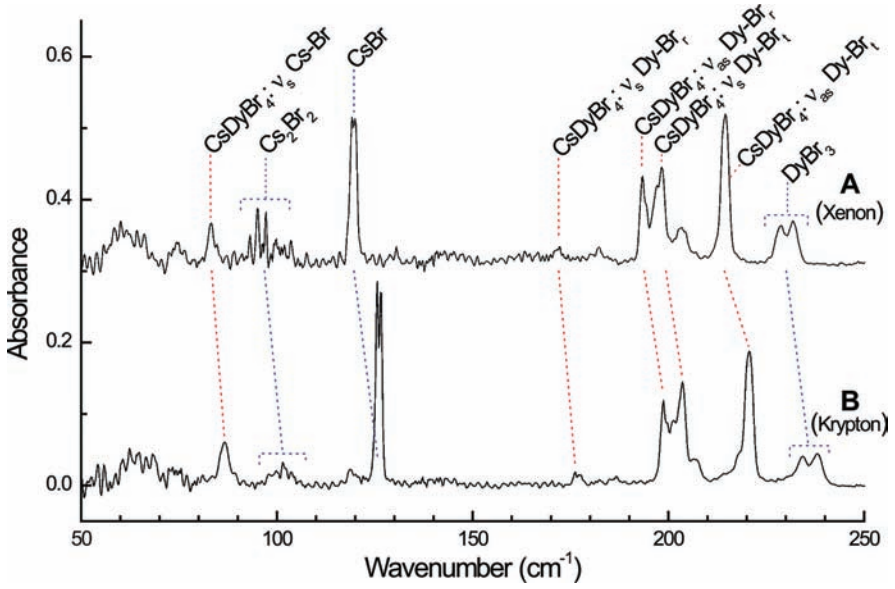

Figure 10. Matrix-isolation IR spectra of CsBr−$DyBr_3$ (molar ratio 5:2) evaporations in Xe and Kr. (A) Xe, 180 min evaporation at T = 960(35) K. (B) Kr, 180 min evaporation at T = 960(35) K.

side of the Cs-X fundamentals (for X = Br at ∼101 cm^{-1} in Kr and at ∼98 cm^{-1} in Xe, and for X = I at ∼85 cm^{-1} in Kr and at ∼78 cm^{-1} in Xe) can be assigned to the B_{2u} and B_{3u} stretching fundamentals of Cs_2X_2.[63]

Also for reference purposes, the spectral characteristics of NaBr and its dimer isolated in xenon have been determined in this study, while the values in krypton have been obtained from the interpolation of the xenon values and the literature values of NaBr isolated in argon.[65] In the matrix-IR spectra of the NaBr−$DyBr_3$ mixture, the NaBr monomer fundamental can be assigned to the signals at 268.9 (Kr) and 259.0 cm^{-1} (Xe). Two additional bands are found in the xenon spectrum which can be assigned to the Na_2Br_2 dimer. These bands are located at 218.2 and 171.8 cm^{-1}. In krypton these bands are found at 225.6/221.8 (split) and at 180.4 cm^{-1}.

In the spectra of the isolated vapors of the CsX−DyX_3 mixtures strong additional signals are present besides the bands already assigned to the binary parent compounds. One band is observed in the Cs−X stretch region, while a group of three strong absorptions is found in the region of Dy−X stretch fundamentals. The four bands show parallel growth behavior and are therefore assigned as belonging to one species. Based

dx.doi.org/10.1021/ic202009v | Inorg. Chem. 2012, 51, 543−556

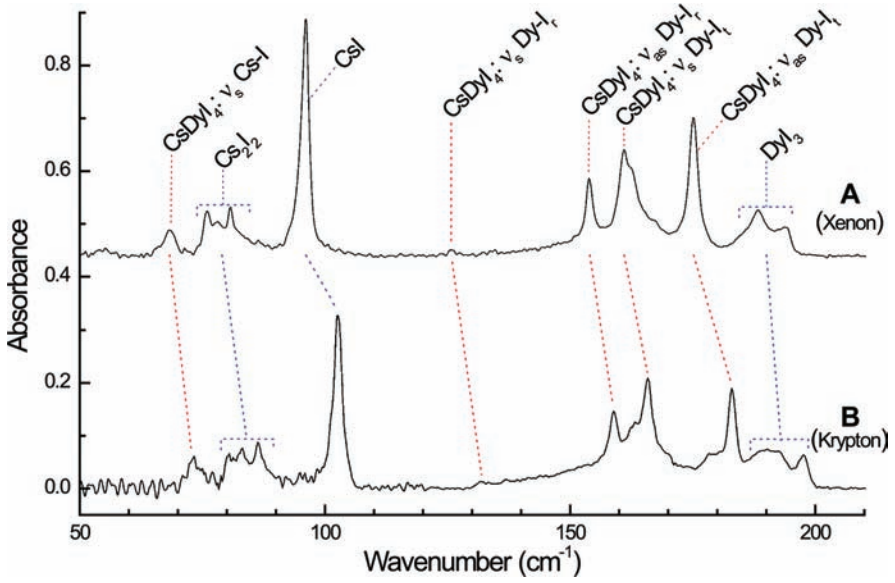

Figure 11. Matrix-isolation IR spectra of CsI−DyI_3 (molar ratio 5:2) evaporations in Xe and Kr. (A) Xe, 135 min evaporation at T = 930(35) K. (B) Kr, 135 min evaporation at T = 935(35) K.

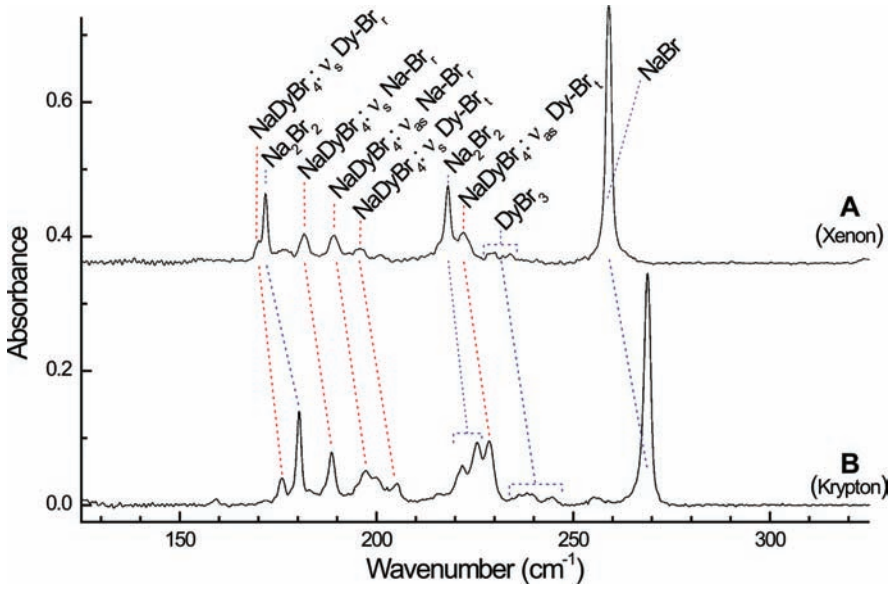

Figure 12. Matrix-isolation IR spectra of NaBr−$DyBr_3$ (molar ratio 3:1) evaporations in Xe and Kr. (A) Xe, 135 min evaporation at T = 980(35) K. (B) Kr, 135 min evaporation at T = 980(35) K.

on the amount of bands in the Dy−X stretching region and the good agreement of the observed band pattern with the computed IR spectrum of the bidentate structure of the $CsDyX_4$ complexes (cf., Figure 9), these four bands are assigned accordingly. Additional proof for the assignment to the bidentate structure is the presence of a very weak signal for X = Br at 176.8 cm^{-1} (Kr) and 171.8 cm^{-1} (Xe) and for X = I at 132.1 (Kr) and 125.8 cm^{-1} (Xe), which originates from the symmetric Dy−X_b stretch. This vibration has an observable infrared intensity only for the bidentate structure; for the tridentate structure it is negligible. The assignment of the main additional bands in the spectrum to the bidentate $CsDyX_4$ complex is also in accordance with the predicted predominance of this isomer in the vapor at the temperature of the experiments (vide supra). The wavenumbers of the $CsDyX_4$ absorptions in krypton and xenon matrices are given in Table 2 and 3 for the experiments on the CsBr−$DyBr_3$ and CsI−DyI_3 mixtures, respectively. The assignment is based on a visual analysis of the atomic displacements in the computed fundamentals using the GaussView 4.1 program and is also shown in Figures 10 and 11.

In case of the NaBr−$DyBr_3$ evaporations, the intensity of the additional signals observed besides the parent compounds is lower as compared to the cesium complexes. Nevertheless, a total of five absorptions could be distinguished in the Dy−X stretching region retaining a more or less constant intensity ratio. Also for $NaDyBr_4$, the observed band pattern is characteristic for the C_{2v} bidentate structure. This observation matches well with the predicted abundance of the bidentate isomer of $NaDyBr_4$ at the temperature of the experiments. The spectral values for the five absorptions of $NaDyBr_4$ are summarized in Table 4 and the assignment is also shown in Figure 12.

dx.doi.org/10.1021/ic202009v | *Inorg. Chem.* 2012, 51, 543−556

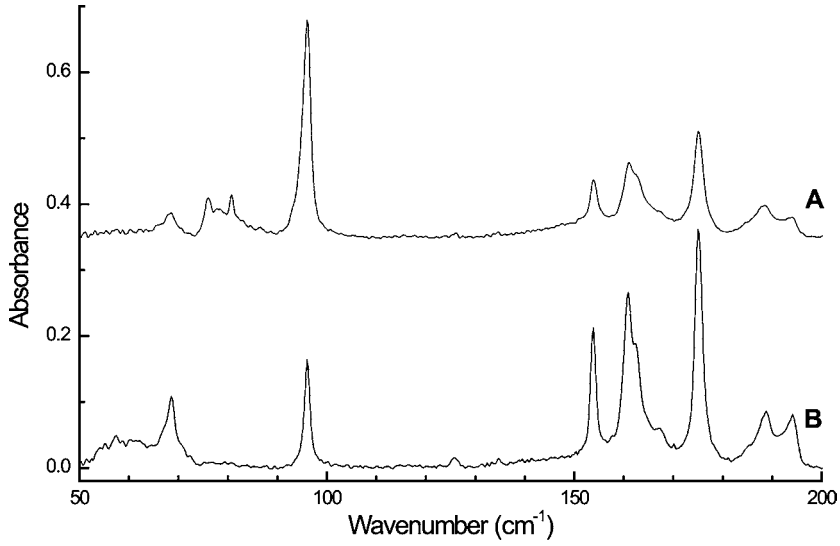

Figure 13. Matrix-isolation IR spectra of 90 min CsI−DyI_3 evaporations at T = 925(30) K in Xe applying different CsI:DyI_3 compositions: (A) CsI:DyI_3 = 5:2 (B) CsI:DyI_3 = 4:3.

Comparing the observed wavenumbers with the computed values for all investigated $MDyX_4$ species shows the expected matrix shift to lower wavenumbers for most fundamentals. The Dy−X_b stretch vibrations are, however, calculated at too low frequencies, as already the krypton values are significantly higher than the computed values, which refer to the gas phase.

The minimum temperature needed for the observation of signals attributable to the $MDyX_4$ complex was lowest for M = Cs, X = I, and highest for M = Na, X = Br, although we have to note that the composition of the latter mixture differed slightly from the other two investigated mixtures (molar ratio was 3:1 instead of 5:2).

An important observation is that the composition of the starting mixture has a significant influence on the relative amounts of the observed vapor species. This is illustrated by selected experiments performed on CsI−DyI_3 mixtures of 4:3 molar ratio as compared to the majority of the results which were obtained on mixtures of 5:2 molar ratio (Figure 13). For the 4:3 CsI−DyI_3 composition, rich in rare earth halide, the signals assigned to the bidentate $CsDyI_4$ complex are much stronger compared to the composition rich in alkali halide. For the 4:3 molar ratio evaporation, the $CsDyI_4$ complex is the most abundant species in the vapor. The Cs_2I_2 dimer signals are absent, while the CsI signal is significantly lower than in case of the alkali rich mixture with composition 5:2. The composition dependence of the amount of the $MDyX_4$ vapor complex has previously been investigated by mass spectroscopy for NaI−DyI_3 mixtures, with results matching the present findings.[66]

In addition to the absorption bands assigned to the bidentate $MDyX_4$ complexes, several low intensity features are observed in the Dy−X stretching region. These are most pronounced in the spectra of the cesium derivatives, as the amount of complex is higher in these experiments than in case of the evaporations of the sodium mixture. Therefore, we have focused with the assignment of these minor bands on the cesium experiments. Generally, the symmetric stretch Dy−X_t signal shows a splitting which disappears upon annealing. This splitting is therefore assigned to a site effect. The symmetric stretch Dy−X_t also contains a shoulder or distinct signal on the high-wavenumber side. Moreover, the antisymmetric stretch Dy−X_t contains for both X = Br, I in krypton a shoulder on the low-wavenumber side. The possibility was considered that both these signals belong to the tridentate isomer, as the computations (see Figure 8) predicted a noticeable amount of tridentate (10−20%) structure present in the vapor at the temperature of our experiments. The computed spectrum of the tridentate isomer consisted of two strong bands in the region of Dy−X stretches. The calculated frequency of the Dy−Br_t stretch fundamental of the tridentate structure was predicted within several reciprocal centimeters of the antisymmetric Dy−Br_t vibration of the bidentate isomer. It is, therefore, well possible that the observed shoulder on the bidentate antisymmetric stretch Dy−X_t band in the krypton matrices belongs to the Dy−Br_t stretch of the tridentate isomer. In the xenon matrices this signal is probably hidden under the bidentate fundamental. The shoulder or distinct signal on the high-wavenumber side of the bidentate symmetric stretch Dy−X_t might very well be the antisymmetric Dy−X_b stretch of the tridentate isomer. In principle, this signal was predicted by the computations to appear in the middle between the antisymmetric Dy−X_b stretch and the symmetric Dy−X_t stretch frequencies of the bidentate structure (see Figure 9), but we already noted that the computations underestimated the Dy−X ring vibrations of the bidentate isomer. If we suppose that the underestimation of the Dy−X ring vibrations probably applies to the computed tridentate fundamentals as well, it may well be possible that the tridentate antisymmetric Dy−X_b stretch appears on the high wavenumber side of the bidentate Dy−X_t signal. The wavenumbers of the tentatively assigned tridentate $CsDyX_4$ absorptions in krypton and xenon matrices are added to Table 2 and 3 for the experiments on the CsBr−$DyBr_3$ and CsI−DyI_3 mixtures, respectively.

According to the computations, the presence of the tridentate isomer in the spectrum would be accompanied by the observation of a band in the region of the Cs−X stretchings as well. The Cs−X symmetric stretch band of the tridentate isomer would appear at ∼10−15 cm^{-1} lower wavenumber than that of the bidentate one, but will almost coincide with the antisymmetric Cs−X stretching of the bidentate isomer. Therefore, the fact that in several spectra we observe a small band in this region (see, for example, Figure 10a, $CsDyBr_4$ in xenon) does not make it possible to prove unambiguously the presence of the tridentate isomer in the vapor. Nevertheless, considering

dx.doi.org/10.1021/ic202009v | Inorg. Chem. 2012, 51, 543−556

our computational results, the presence of the tridentate isomer might be possible. Presuming that during matrix formation the relative abundances of the isomers hardly change, the calculated about 10−20% percent of the tridentate isomer might be expected the same in the matrix as in the gas. On the other hand, if we take into account that, because of the noble gas environment, the energy differences decrease between the isomers, the signals corresponding to the tridentate isomer might eventually disappear from the spectra.

Thermal annealing of the matrices did not result in well-defined changes in the intensity of the tentative tridentate signals with respect to the bidentate model, but do result in several other observations. As can be seen in Figure 14, where

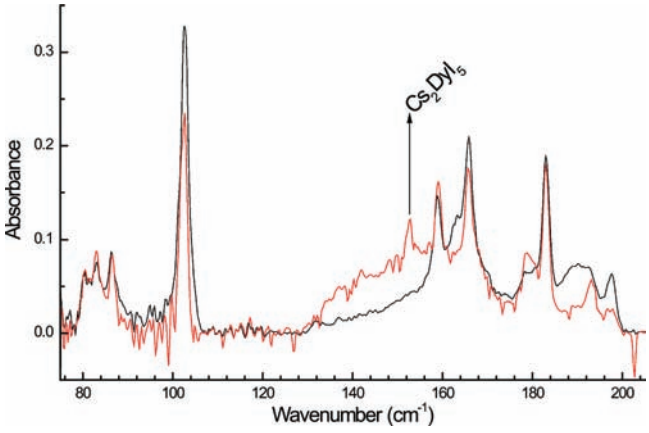

Figure 14. Matrix-isolation IR spectra of a 135 min CsI−DyI_3 (molar ratio 5:2) evaporation at T = 935(35) K in Kr (Black trace). Red trace: after warming up the matrix to 56 K.

an example of an annealing spectrum of a CsI−DyI_3 krypton matrix is given, annealing results in the earlier indicated disappearance of matrix site effects on the signal of DyX_3 and the symmetric stretch Dy−X_t signal of $CsDyX_4$. Also a broad signal appears under the absorptions of $CsDyX_4$, which is usually indicative of aggregation.

On top of the band due to aggregates, a distinct signal grows, which in several concentrated matrices was already present as a very weak signal prior to annealing. From the various possibilities considered for this signal it seems most likely that this signal originates from the double complex M_2DyX_5, which was also detected as a minor vapor species in the mass spectrometric study of several related MX−LnX_3 mixtures (see, for example, ref 2). Computational support for this tentative assignment is not a trivial task as several possible geometries can be proposed for this species. In the Supporting Information a summary of the lowest energy structures and the computed vibrational spectra of the Na_2DyBr_5 and Cs_2DyI_5 species are given. From these, the structure was selected having its strongest vibrational signal computed below the Dy−X signals of the $MDyX_4$ species. The structure resulting in this vibrational spectrum had one alkali atom bound to dysprosium by a tridentate bridge and the other alkali by a bidentate coordination.

CONCLUSIONS

We reported a joint vibrational spectroscopic and computational analysis of $MDyX_4$ complexes (M = Li, Na, K, Rb, Cs; X = F, Cl, Br, I). After testing several theoretical methods considering computational cost and performance, we selected the mPW1PW91 exchange-correlation functional in conjunction with relativistic effective core potentials and cc-pVTZ-quality valence basis sets for the calculations of the geometrical parameters, vibrational frequencies, and thermochemical properties (also at temperatures as high as 1000 K) of all the complexes, their parent molecules, and the related monocations and radicals.

Our calculations predicted the predominance of the bidentate structural isomers at high temperatures, though the most stable structure at 0 K (lacking the effect of entropy) was the tridentate isomer for the heavier halides and alkali metals. The survey of various dissociation processes revealed the preference of the dissociation to neutral MX and DyX_3 fragments over ionic and radical dissociation products. Cationic complexes are considerably less stable at 1000 K than the neutral complexes, and they prefer to dissociate to $M^+ + DyX_4^\bullet$ fragments. In the cationic complexes we discovered a special structural feature: because of the electron depletion on the halogens an X_2Dy triatomic ring is formed with weak halogen−halogen bonding.

The experimental study has been performed on the vapor over mixtures of CsX−DyX_3 (X = Br, I) and NaBr−$DyBr_3$ in the temperature range 900−1000 K. The vapor species have been isolated in krypton and xenon matrices from which the MI-IR spectra have been recorded. Besides the characteristic vibrational frequencies of the monomeric NaBr, CsX and DyX_3 systems and the Na_2Br_2, Cs_2X_2 (X = Br, I) dimers, signals indicating the formation of mixed complexes of stoichiometry $NaDyBr_4$, and $CsDyX_4$ (X = Br, I) have been observed. The absorption pattern of the complexes agrees very well with their computed IR spectra. On the basis of the computed vibrational and thermodynamic data we found the C_{2v}-symmetry bidentate form as the major component in the matrices of the studied complexes. The amount of complex in the vapor strongly depends on the composition of the starting mixture. A composition rich in DyI_3 evaporated in increasing amount as $CsDyI_4$ complex and much less as CsI and Cs_2I_2.

The presence of the tridentate isomer is suggested in the spectra of the cesium derivatives, but it cannot be proved unambiguously. Thermal annealing of the matrices leads to increased aggregation, and the observation of a signal which was tentatively assigned to the double complex, Cs_2DyX_5. From the various possible geometries of this molecule, the computed vibrational spectrum of the species in which one alkali atom is bound to dysprosium by a tridentate bridge, while the other alkali has a bidentate coordination gives the best agreement with the experimental vibrational spectra.

ASSOCIATED CONTENT

Supporting Information

The computed geometrical parameters, vibrational frequencies, enthalpies, entropies, and all other data shown in the figures are given in Tables S1−S24, and the structures, energies, and vibrational frequencies and spectra of Na_2DyBr_5 and Cs_2DyI_5 isomers are given in Tables S25−S27 and Figures S1−S3. This material is available free of charge via the Internet at http://pubs.acs.org.

AUTHOR INFORMATION

Corresponding Author

*E-mail: Attila.Kovacs@ec.europa.eu (A.K.); hargittaim@mail.bme.hu (M.H.).

Present Address

[§]Urenco Nederland B. V., P.O. Box 158, 7600 AD Almelo, The Netherlands

■ ACKNOWLEDGMENTS

This research has been supported by the Hungarian Scientific Research Fund (OTKA K 60365). Computational time from the National Information Infrastructure Development Program of Hungary is gratefully acknowledged. CPG acknowledges the help of Mr. H. Luyten with developing the high temperature furnace for the matrix-isolation setup, and Prof. EHP Cordfunke and Prof. A. Oskam for their helpful comments and suggestions during the experimental phase of this work. The spectroscopic experiments were supported financially by STW (ACH 55.3757) and Philips Lighting B.V.

■ REFERENCES

(1) Boghosian, S.; Papatheodorou, G. N. In *Handbook on the Physics and Chemistry of Rare Earths*; Geschneider, K. A. J., Eyring, L., Eds.; Elsevier: Amsterdam, 1996; Vol. *23*, p 435.
(2) Hilpert, K.; Niemann, U. *Thermochim. Acta* **1997**, *299*, 49−57.
(3) Hilpert, K. *J. Electrochem. Soc.* **1989**, *136*, 2099−2108.
(4) Metallinou, M. M.; Nalbandian, L.; Papatheodorou, G. N.; Voigt, W.; Emons, H. H. *Inorg. Chem.* **1991**, *30*, 4260−4264.
(5) Hilpert, K. In *Struct. Bonding (Berlin)*; Clarke, M. J., Goodenough, J. B., Ibers, J. A., Jorgensen, C. K., Mingos, D. M. P., Neilands, J. B., Palmer, G. A., Reinen, D., Sadler, P. J., Weiss, R., Williams, R. J. P., Eds.; Springer: Berlin, 1990; Vol. *73*, p 97.
(6) Kapala, J.; Roszak, S.; Lisek, I.; Miller, M. *Chem. Phys.* **1998**, *238*, 221−229.
(7) Lisek, I.; Kapala, J.; Miller, M. *J. Alloys Compd.* **1998**, *280*, 77−84.
(8) Hildenbrand, D. L.; Lau, K. H.; Baglio, J. W.; Struck, C. W. *J. Phys. Chem. A* **2005**, *109*, 1481−1486.
(9) Hilpert, K.; Miller, M. *J. Electrochem. Soc.* **1994**, *141*, 2769−2774.
(10) Hilpert, K.; Miller, M. *J. Alloys Compd.* **2004**, *379*, 1−7.
(11) Papatheodorou, G. N.; Chrissanthopoulos, A. *J. Mol. Struct.* **2007**, *832*, 38−47.
(12) Schäfer, H. *Angew. Chem., Int. Ed. Engl.* **1976**, *15*, 713−727.
(13) Papatheodorou, G. N. In *Current Topics in Materials Science*; Kaldis, E., Ed.; North-Holland: Amsterdam, 1982; Vol. *10*.
(14) Schäfer, H. *Adv. Inorg. Chem.* **1983**, *26*, 201−234.
(15) Hastie, J. W. *High Temperature Vapors*; Academic Press: New York, 1975.
(16) Murase, K.; Machida, K.; Adachi, G. *J. Alloys Compd.* **1995**, *217*, 218−225.
(17) Murase, K.; Adachi, G.; Hashimoto, M.; Kudo, H. *Bull. Chem. Soc. Jpn.* **1996**, *69*, 353−357.
(18) Feltrin, A.; Cesaro, S. N. *High Temp. Mater. Sci.* **1996**, *35*, 203−214.
(19) Spiridonov, V. P.; Brezgin, Y. A.; Shakhparonov, M. I. *Zh. Strukt. Khim.* **1971**, *12*, 1080.
(20) Hargittai, M. *Chem. Rev.* **2000**, *100*, 2233−2301.
(21) Kapala, J.; Lisek, I.; Roszak, S.; Miller, M. *Polyhedron* **1999**, *18*, 2845−2851.
(22) Groen, P.; Oskam, A.; Kovács, A. *J. Mol. Struct. (THEOCHEM)* **2000**, *531*, 23−31.
(23) Groen, C. P.; Oskam, A.; Kovács, A. *Inorg. Chem.* **2000**, *39*, 6001−6008.
(24) Groen, C. P.; Oskam, A.; Kovács, A. *Inorg. Chem.* **2003**, *42*, 851−858.
(25) Varga, Z.; Hargittai, M. *Struct. Chem.* **2006**, *17*, 225−233.
(26) Liebman, J. F.; Varga, Z.; Hargittai, M. *Struct. Chem.* **2007**, *18*, 269−271.
(27) Becke, A. D. *J. Chem. Phys.* **1993**, *98*, 5648−5652.
(28) Lee, C.; Yang, W.; Parr, R. G. *Phys. Rev. B* **1988**, *37*, 785−789.
(29) Perdew, J. P.; Chevary, J. A.; Vosko, S. H.; Jackson, K. A.; Pederson, M. R.; Singh, D. J.; Fiolhais, C. *Phys. Rev. B* **1992**, *46*, 6671−6687.
(30) Adamo, C.; Barone, V. *J. Chem. Phys.* **1998**, *108*, 664−675.
(31) Møller, C.; Plesset, M. S. *Phys. Rev.* **1934**, *46*, 618−622.
(32) Dolg, M. Ph.D. Thesis, University of Stuttgart, 1989.
(33) Dolg, M.; Stoll, H.; Savin, A.; Preuss, H. *Theor. Chim. Acta* **1989**, *75*, 173−194.
(34) Dolg, M.; Stoll, H.; Preuss, H. *Theor. Chim. Acta* **1993**, *85*, 441−450.
(35) Dunning, T. H. Jr. *J. Chem. Phys.* **1989**, *90*, 1007−1023.
(36) Woon, D. E.; Dunning, T. H., Jr. Unpublished, available at the web site of EMSL Basis Set Exchange (https://bse.pnl.gov/bse/portal).
(37) Woon, D. E.; Dunning, T. H. J. *J. Chem. Phys.* **1993**, *98*, 1358−1371.
(38) Bergner, A.; Dolg, M.; Kuchle, W.; Stoll, H.; Preuss, H. *Mol. Phys.* **1993**, *80*, 1431−1441.
(39) Martin, J. M. L.; Sundermann, A. *J. Chem. Phys.* **2001**, *114*, 3408−3420.
(40) Lim, I. S.; Schwerdtfeger, P.; Metz, B.; Stoll, H. *J. Chem. Phys.* **2005**, *122*, 104103.
(41) Groen, C. P.; Varga, Z.; Kolonits, M.; Peterson, K. A.; Hargittai, M. *Inorg. Chem.* **2009**, *48*, 4143−4153.
(42) Giricheva, N. I.; Shlykov, S. A.; Chernova, E. V.; Levina, Y. S.; Krasnov, A. V. *Russ. J. Struct. Chem.* **2005**, *46*, 1031−1037.
(43) Frisch, M. J.; Trucks, G. W.; Schlegel, H. B.; Scuseria, G. E.; Robb, M. A.; Cheeseman, J. R.; Zakrzewski, V. G.; Jr, J., A. M.; Stratmann, R. E.; Burant, J. C.; Dapprich, S.; Millam, J. M.; Daniels, A. D.; Kudin, K. N.; Strain, M. C.; Farkas, O.; Tomasi, J.; Barone, V.; Cossi, M.; Cammi, R.; Mennucci, B.; Pomelli, C.; Adamo, C.; Clifford, S.; Ochterski, J.; Petersson, G. A.; Ayala, P. Y.; Cui, Q.; Morokuma, K.; Rabuck, A. D.; Raghavachari, K.; Foresman, J. B.; Cioslowski, J.; Ortiz, J. V.; Stefanov, B. B.; Liu, G.; Liashenko, A.; Piskorz, P.; Komaromi, I.; Gomperts, R.; Martin, R. L.; Fox, D. J.; Keith, T.; Al-Laham, M. A.; Peng, C. Y.; Nanayakkara, A.; Gonzalez, C.; Challacombe, M.; Gill, P. M. W.; Johnson, B.; Chen, W.; Wong, M. W.; Andres, J. L.; Gonzalez, C.; Head-Gordon, M.; Replogle, E. S.; Pople, J. A. *Gaussian 98*, revision A.5; Gaussian Inc.: Pittsburgh PA, 1998.
(44) Frisch, M. J.; Trucks, G. W.; Schlegel, H. B.; Scuseria, G. E.; Robb, M. A.; Cheeseman, J. R.; Montgomery Jr., J. A.; Vreven, T.; Kudin, K. N.; Burant, J. C.; Millam, J. M.; Iyengar, S. S.; Tomasi, J.; Barone, V.; Mennucci, B.; Cossi, M.; Scalmani, G.; Rega, N.; Petersson, G. A.; Nakatsuji, H.; Hada, M.; Ehara, M.; Toyota, K.; Fukuda, R.; Hasegawa, J.; Ishida, M.; Nakajima, T.; Honda, Y.; Kitao, O.; Nakai, H.; Klene, M.; Li, X.; Knox, J. E.; Hratchian, H. P.; Cross, J. B.; Bakken, V.; Adamo, C.; Jaramillo, J.; Gomperts, R.; Stratmann, R. E.; Yazyev, O.; Austin, A. J.; Cammi, R.; Pomelli, C.; Ochterski, J. W.; Ayala, P. Y.; Morokuma, K.; Voth, G. A.; Salvador, P.; Dannenberg, J. J.; Zakrzewski, V. G.; Dapprich, S.; Daniels, A. D.; Strain, M. C.; Farkas, O.; Malick, D. K.; Rabuck, A. D.; Raghavachari, K.; Foresman, J. B.; Ortiz, J. V.; Cui, Q.; Baboul, A. G.; Clifford, S.; Cioslowski, J.; Stefanov, B. B.; Liu, G.; Liashenko, A.; Piskorz, P.; Komaromi, I.; Martin, R. L.; Fox, D. J.; Keith, T.; Al-Laham, M. A.; Peng, C. Y.; Nanayakkara, A.; Challacombe, M.; Gill, P. M. W.; Johnson, B.; Chen, W.; Wong, M. W.; Gonzalez, C.; Pople, J. A. *Gaussian 03*, revision B.05 ed.; Gaussian Inc.: Pittsburgh, PA, 2003.
(45) Hilpert, K.; Miller, M. *High Temp.−High Press.* **1988**, *20*, 231.
(46) Stevens, W. J.; Krauss, M.; Basch, H.; Jasien, P. G. *Can. J. Chem.* **1992**, *70*, 612−630.
(47) The origonal Cundari-Stevens basis set of Dy was extended by one g = 1.4 exponent.
(48) Frisch, M. J.; Trucks, G. W.; Schlegel, H. B.; Scuseria, G. E.; Robb, M. A.; Cheeseman, J. R.; Scalmani, G.; Barone, V.; Mennucci, B.; Petersson, G. A.; Nakatsuji, H.; Caricato, M.; Li, X.; Hratchian, H. P.; Izmaylov, A. F.; Bloino, J.; Zheng, G.; Sonnenberg, J. L.; Hada, M.; Ehara, M.; Toyota, K.; Fukuda, R.; Hasegawa, J.; Ishida, M.; Nakajima, T.; Honda, Y.; Kitao, O.; Nakai, H.; Vreven, T.; Montgomery, J., J. A.; Peralta, J. E.; Ogliaro, F.; Bearpark, M.; Heyd, J. J.; Brothers, E.; Kudin, K. N.; Staroverov, V. N.; Kobayashi, R.; Normand, J.; Raghavachari, K.;

Rendell, A.; Burant, J. C.; Iyengar, S. S.; Tomasi, J.; Cossi, M.; Rega, N.; Millam, N. J.; Klene, M.; Knox, J. E.; Cross, J. B.; Bakken, V.; Adamo, C.; Jaramillo, J.; Gomperts, R.; Stratmann, R. E.; Yazyev, O.; Austin, A. J.; Cammi, R.; Pomelli, C.; Ochterski, J. W.; Martin, R. L.; Morokuma, K.; Zakrzewski, V. G.; Voth, G. A.; Salvador, P.; Dannenberg, J. J.; Dapprich, S.; Daniels, A. D.; Farkas, Ö.; Foresman, J. B.; Ortiz, J. V.; Cioslowski, J.; Fox, D. J. *Gaussian 09*, revision B.01 ed.; Gaussian Inc.: Wallingfort, CT, 2010.

(49) Kobertz, D.; Hilpert, K.; Kapala, J.; Miller, M. *Calphad* **2004**, *28*, 203−208.

(50) Huntelaar, M. E.; Cordfunke, E. H. P. Thermodynamisch onderzoek en berekeningen aan het systeem CsI−CsBr−DyI_3−$DyBr_3$, ECN-C−97-038, 1997.

(51) Klotzbücher, W. E. *Cryogenics* **1983**, *23*, 554−556.

(52) Klotzbücher, W. E. Personal communication.

(53) *CRC Handbook of Chemistry and Physics*, 83rd ed.; Lide, D. R., Ed.; CRC Press: Boca Raton, FL, U.S.A., 2002.

(54) Saloni, J.; Roszak, S.; Hilpert, K.; Miller, M.; Leszczynski, J. *Eur. J. Inorg. Chem.* **2004**, 1212−1218.

(55) Saloni, J.; Roszak, S.; Hilpert, K.; Popovic, A.; Miller, M.; Leszczynski, J. *Inorg. Chem.* **2006**, *45*, 4508−4517.

(56) Biegler-Konig, F.; Schonbohm, J.; Bayles, D. *J. Comput. Chem.* **2001**, *22*, 545−559.

(57) Biegler-Konig, F.; Schonbohm, J. *J. Comput. Chem.* **2002**, *23*, 1489−1494.

(58) *CRC Handbook of Chemistry and Physics*, 84th ed.; Lide, D. R., Ed.; CRC Press.: Boca Raton, FL, U.S.A., 2003.

(59) Arthers, S. A.; Beattie, I. R.; Jones, P. J. *J. Chem. Soc., Dalton Trans.* **1984**, 711−713.

(60) Beattie, I. R.; Millington, K. R. *J. Chem. Soc., Dalton Trans.* **1987**, 1521−1527.

(61) Onsager, L. *J. Am. Chem. Soc.* **1936**, *58*, 1486−1493.

(62) Wong, M. W.; Wiberg, K. B.; Frisch, M. J. *J. Am. Chem. Soc.* **1992**, *114*, 1645−1652.

(63) Groen, C. P.; Kovacs, A. *Vib. Spectrosc.* **2010**, *54*, 30−34.

(64) Varga, Z.; Groen, C. P.; Kolonits, M.; Hargittai, M. *Dalton Trans.* **2010**, *39*, 6221−6230.

(65) Martin, T. P.; Schaber, H. *J. Chem. Phys.* **1978**, *68*, 4299−4303.

(66) Hilpert, K.; Miller, M.; Gerads, H.; Saha, B. *Ber. Bunsen. Phys. Chem.* **1990**, *94*, 35−39.